JOURNAL OF Applied Polymer SCIENCE

Structure and Property of Tetrafluoroethylene-Propylene Elastomer-OVPOSS Composites

Cong Chuanbo, Cui cancan, Meng Xiaoyu, Zhou Qiong
Beijing Key Laboratory of Failure, Corrosion and Protection of Oil/gas Facilities, Department of Material Science and Engineering, China University of Petroleum (Beijing), Beijing 102249, China
Correspondence to: C. Chuanbo (E-mail: occb@163.com)

ABSTRACT: Tetrafluoroethylene-propylene elastomer-octavinyl-polyhedral oligomeric silsesquioxane (TFE/P-OVPOSS) composites containing various percentages of OVPOSS are prepared via room temperature milling and heat vulcanization at 170°C. The composites are characterized by FTIR, ^{13}C-NMR, ^{29}Si-NMR, XRD, DSC, SEM, tensile test, DMA, and TGA. The crosslink bond formation between TFE/P and OVPOSS conforms to the structural characterization of the composites. The OVPOSS cages aggregate when the OVPOSS dosage is more than 6 as observed from the XRD curves and SEM images. The swelling test shows that the experimental crosslink density is lower than the calculated crosslink density, indicating that not all reacted vinyl groups are converted into crosslink bonds. Meanwhile, the incorporation of OVPOSS significantly enhances the mechanical property and elevates the glass temperature of the composites. However, the thermal property is only improved slightly. © 2013 Wiley Periodicals, Inc. J. Appl. Polym. Sci. 130: 1281–1288, 2013

KEYWORDS: composites; crosslinking; elastomers; structure-property relations

Received 11 November 2012; accepted 28 February 2013; published online 24 April 2013
DOI: 10.1002/app.39223

INTRODUCTION

Tetrafluoroethylene-propylene (TFE/P) copolymer is a type of elastomer with a unique combination of high temperature, electrical, and chemical resistance properties.[1,2] Applications of TFE/P have now emerged in corrosive oilfield environments and in the general, chemical, agrichemical, automotive, and aerospace industries.[3]

TFE/P copolymer has no cure sites and is chemically stable. It cannot be cured by most crosslink agents, including polyamines and polyhydroxyaromatics. However, it is only slightly susceptible to peroxide at high temperatures.[4] Some coagents, such as triallyl cyanurate(TAC) and triallyl isocyanurate(TAIC), are necessary to obtain good mechanical properties during peroxide vulcanization.[4] These coagents have the same characteristics that several double bonds exist in the molecule structure. Thus, stable crosslink bonds between the coagent and the macromolecule main chain can form through these double bonds.

Polyhedral oligomeric silsesquioxanes (POSS), with the general formula (RSiO3/2)n (n = 6,8,10…14),[5–7] is a nanometer-sized hybrid material that provides a better choice for preparing nanocomposites through copolymerization,[8,9] grafting,[10–12] or blending.[13–16] Several studies found reinforcements in the thermal stability[8,17,18] and mechanical properties[19,20] of composite materials. However, the effects of POSS fillers on material properties depend substantially on the interactions between POSS and the polymer matrix. The strong interaction can improve the reinforcement effect of the composite. Octavinyl polyhedral oligomeric silsesquioxane (OVPOSS) has eight double bonds that can react with TFE/P elastomer and endow the strong interaction with each other. Meanwhile, OVPOSS can act as a coagent and filler-reinforcing agent for TFE/P elastomer because of the high bond energy of the Si—O bond and its nanometer effect. Thus, OVPOSS can act as a coagent in TFE/P elastomer.

In this paper, TFE/P elastomer-OVPOSS composites were prepared using a peroxide vulcanizing system. The structures of the composites were characterized by IR spectroscopy, ^{13}C-NMR, ^{29}Si-NMR, and X-ray diffraction (XRD). Their mechanical and thermal properties were measured by tensile experiment, thermogravimetric analysis (TGA), and dynamic mechanical analysis (DMA).

EXPERIMENT

Materials

TFE/P (Aflas® 100S) was supplied by Japan Asahi Glass (Tokyo, Japan). OVPOSS (purity> 99%) supplied by Shenyang Amwest Technology Company (Shenyang, Liaoning) was used as the auxiliary crosslinking agent for the TFE/P rubber. Dicumyl peroxide (DCP, purity > 99%) supplied by Kunshan Yalong Trading (Jiangsu, China) was used as the main crosslinking agent

for the TFE/P rubber. Ethyl acetate (purity> 99%) supplied by Beijing Chemical Works (Beijing, China) was used as the swelling solvent for measuring the crosslink density. Other materials were of industrial grade and were used as received.

Preparation of TFE/P Elastomer-OVPOSS Composites

Raw TFE/P (100 g) was softened by passing several times through a rubber mill (XK-160, Qingdao Tycoon International Trade, China), mixed with various OVPOSS loadings (2, 4, 6, 8, and 10 g) and 4 g of DCP, and then vulcanized in a rubber mold machine (QLB-600, Nantong Atlantic Machinery, China) at 170°C and 10 MPa for 15 min. The obtained vulcanized rubbers were assigned as POSS-2, POSS-4, POSS-6, POSS-8, and POSS-10.

MEASUREMENTS AND CHARACTERIZATIONS

Attenuated Total Reflectance Fourier-Transform Infrared (ATR-FTIR) Spectroscopy

Infrared spectra of the solid samples were obtained at room temperature with a Nicolet Nexus 670 ATR-FTIR spectrometer. Single beam spectra of the samples were obtained after an average of 40 scans between 4000 and 500 cm^{-1} with a resolution of 2 cm^{-1}. All spectra were obtained in the transmittance mode.

^{13}C- and ^{29}Si-NMR Spectroscopy

Solid state NMR was conducted at room temperature on a BrukerAV600 spectrometer operating at 600 MHz. The samples were run in a MAS rotor 4 mm in diameter (internal diameter: 3.7 mm) and 10 mm in length. Approximately 10 mg of the samples was added at a time and pressed into the rotor with a metallic tool. The MAS spinning rate was 10,000 Hz, the 90° pulse width was 3.7 μs, and the ramped CP pulse was 1 ms. The signals between −25 and 200 ppm for ^{13}C-NMR and between −100 and −45 ppm for ^{29}Si-NMR were analyzed to distinguish the different carbon and silicon atoms.

DMA

A Netzsch equipment (DMA242, NETZSCH Company, Germany) was used in tensile mode at an oscillatory frequency of 10 Hz with 1% applied strain for all samples. The temperature scan was performed at 3°C/min heating rate in the range of −60°C to 80°C for all composites. Sample dimensions were typically 40 mm long, 4 mm wide, and approximately 2 mm thick.

Tensile Test

Sample sheets were cut into standard GB/T 528 dog bone-shaped test specimens (cross-section 4 mm × 2 mm). The tensile tests were carried out on a tensile machine model WDL-50 at an extension rate of 500 mm/min at room temperature (~23°C). Five specimens of each composite were tested. The results were averaged, and standard deviations were reported.

TGA

The thermal stability of the samples was measured by TGA using a Shimadzu DTG-60 thermogravimetric analyzer. The sample weight was ~5 mg. Weight loss was recorded as the samples were heated at a rate of 10°C/min from room temperature to 600°C under a dry nitrogen purge of 40 mL/min.

Wide-Angle X-Ray Diffraction (WAXD)

WAXD was carried out at room temperature on an X-ray diffractometer in normal reflection mode with Ni-filtered Cu K_α radiation (λ=1.54 Å). The 2θ scan data were collected at an interval of 0.02°, a scan speed of 2° (2θ)/min, and a scan range of 5° to 30° (2θ).

Scanning Electron Microscopic (SEM) Characterization

The micromorphologies of the composites were investigated by SEM on Quanta 200F SEM. The fracture surfaces of the specimens were coated with gold by vapor deposition using a Denton Desk-1 vacuum sputter coater for SEM observation.

Determination of Crosslink Density

Equilibrium swelling was used to determine the crosslink density of the vulcanizates.[21] Samples were swollen in ethyl acetate at room temperature for 72 h and then removed from the solvent. The surface ethyl acetate was quickly blotted off. The samples were immediately weighed, dried in a vacuum oven for 36 h at 80°C to remove completely the solvent, and then reweighed. The volume fraction of TFE/P in the swollen gel, V_r, was calculated as follows:

$$V_r = \frac{m_0\phi(1-\alpha)/\rho_r}{m_0(1-\alpha)/\rho_r + (m_2-m_1)/\rho_s} \quad (1)$$

where m_0 is the sample mass before swelling, m_1 and m_2 are the sample masses before and after drying, respectively, ϕ is the mass fraction of the rubber in the vulcanizate, α is the mass loss of the gum TFE/P vulcanizate during swelling, and ρ_r and ρ_s are the rubber and solvent densities, respectively.

The elastically network chain density, V_e, which was used to represent the crosslink density, was calculated using the well-known Flory–Rehner equation:

$$V_e = -\frac{\ln(1-V_r) + V_r + \chi V_r^2}{V_s(V_r^{1/3} - V_r/2)} \quad (2)$$

where V_r is the volume fraction of the polymer in the vulcanizate swollen to equilibrium, V_s is the solvent molar volume (98 cm^3/mol for ethyl acetate), and χ is the TFE/P–ethyl acetate interaction parameter calculated as 0.498 from the OVPOSS-2 experimental data.

Differential Scanning Calorimetry Analyses

Differential scanning calorimetry (DSC) measurements were carried out using a differential scanning calorimeter (Netzsch 204F1) equipped with an intracooler and supported by a computer for data acquisition and analysis. The instrument was calibrated using the melting point of high-purity indium. All experiments were conducted under a dry nitrogen flow of 20 mL/min as purge gas. Approximately 5 mg to 10 mg of the samples was enclosed in aluminum DSC capsules. The temperature scan for all composites was performed at 3°C/min heating rate in the range of −50°C to 50°C.

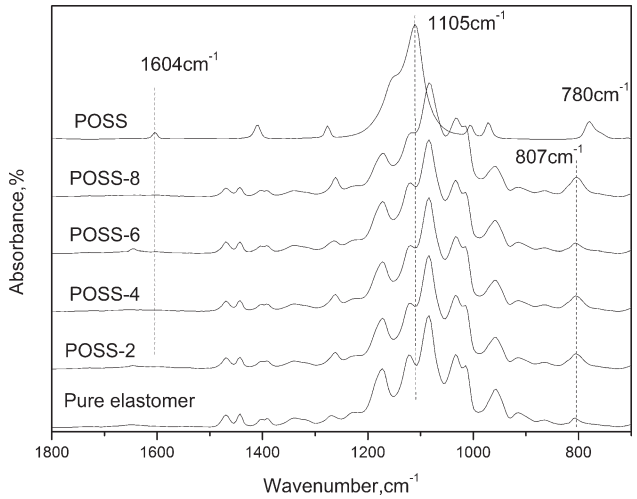

Figure 1. FTIR spectrum of the TFE/P-OVPOSS composites with different contents.

RESULTS AND DISCUSSION

Structural Characterization of the Composites with Different OVPOSS Contents

The FTIR spectrum of the TFE/P-OVPOSS composites is shown in Figure 1. In contrast to pure elastomer, several characteristic peaks of OVPOSS overlap with that of pure elastomer. Hence, distinguishing the characteristic peaks of OVPOSS from the spectrum of the composites is difficult. However, the spectrum of the composites with different OVPOSS contents shows that the absorbance intensities of Si—O—Si and Si—C at 1105 and 807 cm^{-1} slightly increase with increasing OVPOSS content. The absorbance peak of OVPOSS at 1604 cm^{-1} is attributed to the vinyl group,[22,23] which does not appear in the spectrum of the TFE/P-OVPOSS composites. This result suggests that most vinyl groups of OVPOSS participate in the crosslink reaction with TFE/P or that the addition of 8 phr OVPOSS to the rubber cannot change the composite spectra at 1604 cm^{-1}. For FTIR analysis precision, more details about the crosslink reaction are not found. Thus, NMR experiments are conducted.

The ^{13}C-NMR spectra of the composites with different OVPOSS contents are shown in Figure 2(A). The intensities of the peaks at 128 and 137 ppm increase with OVPOSS content. The two peaks are the α- and β-carbon of the vinyl group of OVPOSS. The peak at 13 ppm is attributed to methyl carbon, whereas that at 30.4 ppm is ascribed to the carbon of ethylene and methine groups. However, compared with the neat rubber, a new peak is observed at 25 ppm due to crosslink bond formation. ^{29}Si-NMR analysis [Figure 2(B)] is conducted to prove the reaction of the vinyl group of OVPOSS with TFE/P. A narrow peak of the neat OVPOSS is observed at −80 ppm; this peak is attributed to the silicon atom connected with the vinyl groups.[24] This peak becomes broader on the composite spectra, indicating that the chemical situation of Si becomes versatile because the number of remnant vinyl groups on each OVPOSS cage is different. Moreover, one new broad peak is observed at −66 ppm. This peak, which is attributed to the atom connected with a saturated group, implies crosslink bond formation.[24]

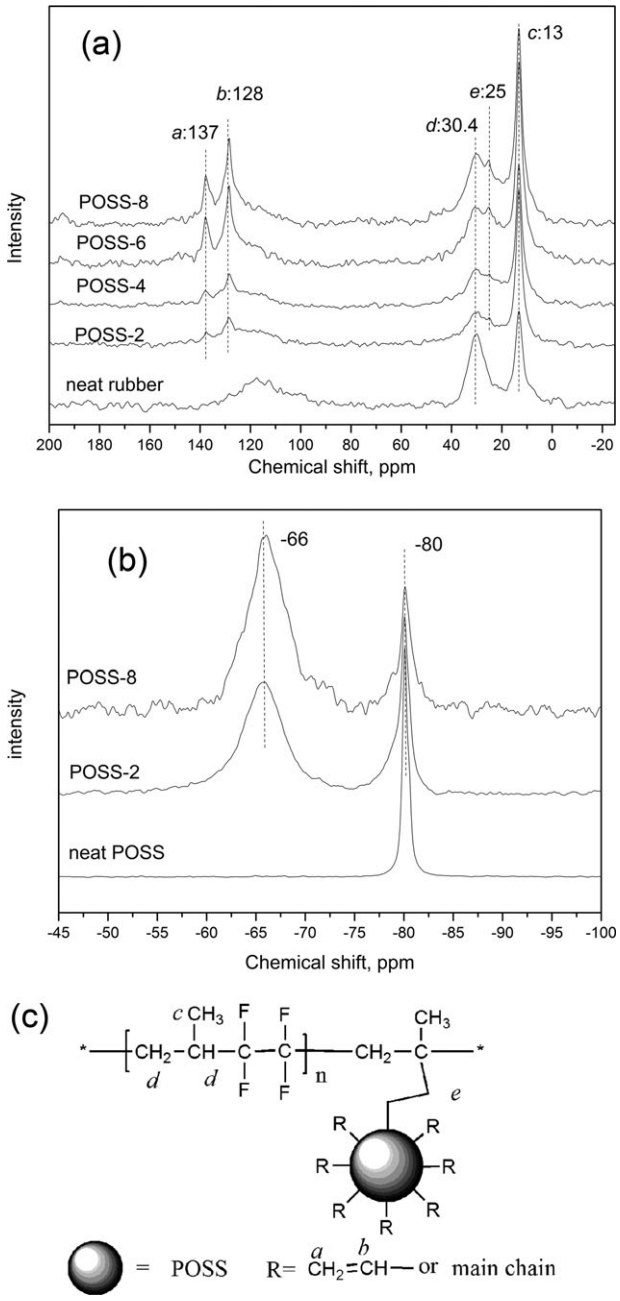

Figure 2. ^{13}C-NMR (a) and ^{29}Si-NMR (b) of the TFE/P-OVPOSS composites with different OVPOSS contents and molecular structure (c).

Based on the area ratios of two peaks at −80 and −66 ppm, the vinyl group utilization is 6.2 for every eight vinyl groups of one OVPOSS molecule in POSS-2. Although the utilization of POSS-8 slightly decreases, it becomes ~5.3 for every eight vinyl groups of one OVPOSS molecule. This utilization ratio is much lower than that reported in the literature.[25,26] This discrepancy may be attributed to the high OVPOSS content.

The structures of the neat POSS and composites with different OVPOSS contents are also characterized by XRD measurements. As shown in Figure 3, the neat OVPOSS has sharp crystalline peaks at 2θ = 9.8°, 13.1°, 19.6°, 21°, 22.8°, 23.7°. This finding

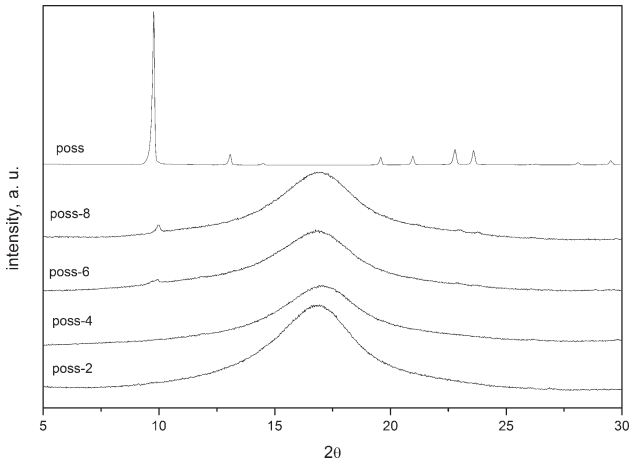

Figure 3. XRD curves of the TFE/P-OVPOSS composites with different OVPOSS contents.

is in close agreement with the literature results for OVPOSS structure.[27] POSS-2 and POSS-4 demonstrate irregular curves resulting from the diffused amorphous TFE/P chains, and no characteristic diffraction peak of the OVPOSS crystalline is found. This result suggests that OVPOSS cages are well dispersed in the polymer matrix. However, one characteristic diffraction peak of POSS cage at $2\theta = 9.8°$ is observed on the POSS-6 and POSS-8 curves, indicating the aggregation of OVPOSS cages. The crystalline structure of the aggregated cages is the same as that of the neat OVPOSS.

The number of vinyl groups per unit volume can be obtained using eq. (3). All vinyl groups that participate in the chemical reaction are assumed to be converted into crosslink bonds during heat vulcanization. Thus, the vinyl group density is equal to the crosslink density, which is theoretical.

$$V_t = \frac{m_1/M_1}{(m_1 + m_2 + m_3)/\rho_c} \times \eta \qquad (3)$$

where V_t represents the theoretical crosslink density; m_1, m_2, and m_3 are the weights of POSS, TFE/P (100 g), and DCP (4 g), respectively; M_1 is the molecular weight of POSS (633 g/mol); ρ_c is the density of the TFE-P/OVPOSS composites; and η is the conversion rate of the vinyl group, which can be obtained from the ^{29}Si-NMR spectra.

The ^{29}Si-NMR spectra show that the conversion rates of the vinyl groups of POSS-2 and POSS-8 are 81.3% (6.5/8) and 66.3% (5.3/8), respectively. The conversion rate is assumed to be proportional to POSS content. Thus, the vinyl group conversion rates of POSS-4 and POSS-6 can be obtained. Subsequently, the theoretical crosslink densities of the composites can be obtained (Table I).

The interaction parameter of the composite-ethyl acetate is necessary to obtain the experimental crosslink density of the composites. However, this interaction parameter is not available from the information we retrieved. Thus, we try to suppose one interaction parameter based on the following theory. The OVPOSS cages in POSS-2 with low OVPOSS content is far from and hardly touch each other. This condition indicates that all reaction vinyl groups are converted into crosslink bonds and that no aggregation occurs between the OVPOSS cages, which can be concluded from the XRD results. Thus, the calculated crosslink density of POSS-2 can be considered as its theoretical value. Using this value and the Flory-Rehner equation, the interaction parameter of the composite and ethyl acetate is 0.498. With this parameter and equation, the experimental crosslink densities of the other composites can be obtained (Table I).

Figure 4 shows the dependence of the experimental and theoretical crosslink densities on POSS content. Both experimental and theoretical values increase with increasing POSS content. However, the experimental value curve against the POSS content does not match with the theoretical value curve. The experimental values of crosslink density are significantly lower than the theoretical values. This result implies that not all reaction vinyl groups are converted into efficient crosslink bonds. Some are converted into a certain alkyl group, which loses reaction activity. The more OVPOSS is added, the more alkyl group is converted. Therefore, the vinyl groups of OVPOSS during vulcanization are divided into three categories: (A) unreacted group, (B) those that form crosslinks, and (C) those that are converted into alkyl groups whose signals cannot be distinguished from the peak *e* in the ^{29}Si-NMR spectra.

Figure 5 shows the SEM images of the fractured surface of the TFE/P-POSS composites with different OVPOSS loadings. The fraction surfaces of the composites become more rugged with increasing OVPOSS loading. This result suggests that the interfacial bonding between the OVPOSS cages and TFE/P increases.

Table I. Experimental and Theoretical Crosslink Densities of the TFE/P-POSS Composites

	POSS-2	POSS-4	POSS-6	POSS-8
Weight of POSS (m_1), g	2	4	6	8
Density of TFEP-POSS composite (ρ_c), g/cm^3	1.522	1.520	1.516	1.516
Conversion rate of vinyl group, %	81.3	76.3[a]	71.3[a]	66.3
Conversion amount of vinyl groups, mol*10^{-3}	2.57	4.82	6.76	8.38
Theoretical crosslink density of composite (V_t), mol/cm^3 10^{-4}	2.86	5.43	7.46	9.07
Experimental crosslink density of composite (V_e), mol/cm^3 10^{-4}[b]	2.86	4.6	5.16	5.7

[a]The value is calculated.
[b]The calculated composite-ethyl acetate interaction parameter is 0.498.

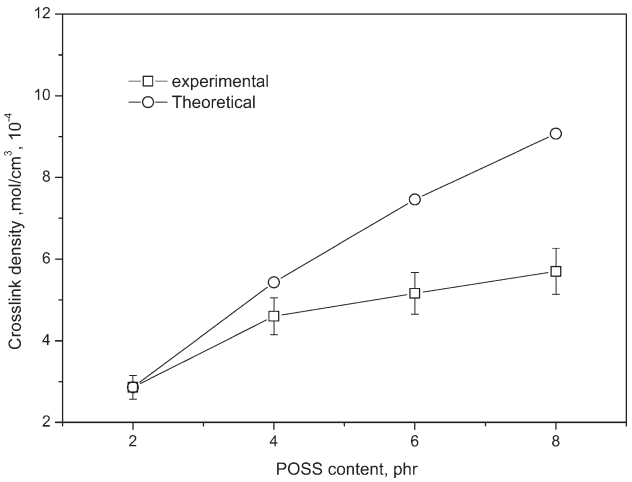

Figure 4. Experimental and theoretical crosslink densities of the TFE/P-OVPOSS composites with different OVPOSS contents.

Moreover, the OVPOSS cages are well dispersed in the polymer matrix for POSS-2, POSS-4, and POSS-6. Shadows are also observed around the particles. However, the XRD curve shows that the particles of POSS-6 aggregate, which may be attributed to the high sensibility of this composite. The aggregated particles of POSS-8 are obviously larger than those of the composites with lower OVPOSS loadings because of the aggregation of OVPOSS.

Mechanical and Thermal Properties of the TFE/P-POSS Composites with Different OVPOSS Loadings

The mechanical properties of the TFE/P-POSS composites are shown in Figure 6. OVPOSS has a significant reinforcement effect on TFE/P elastomer. With increasing OVPOSS loading, the hardness and ultimate tensile strength increase progressively and the elongation at break of the composites simultaneously decreases. The change trend of the tensile strength of the composites is similar to that of the crosslink density. This result suggests that crosslink density has a significant effect on the poperties of the composites with different contents. The aggregation of the OVPOSS cages is less helpful in reinforcing the mechanical properties of the composites.

Figure 7 shows the TGA thermograms of various TFE/P-POSS composites, pure rubber, and pure POSS. The temperatures of 5% weight loss (T_{dec}) and the char yield are recorded in Table

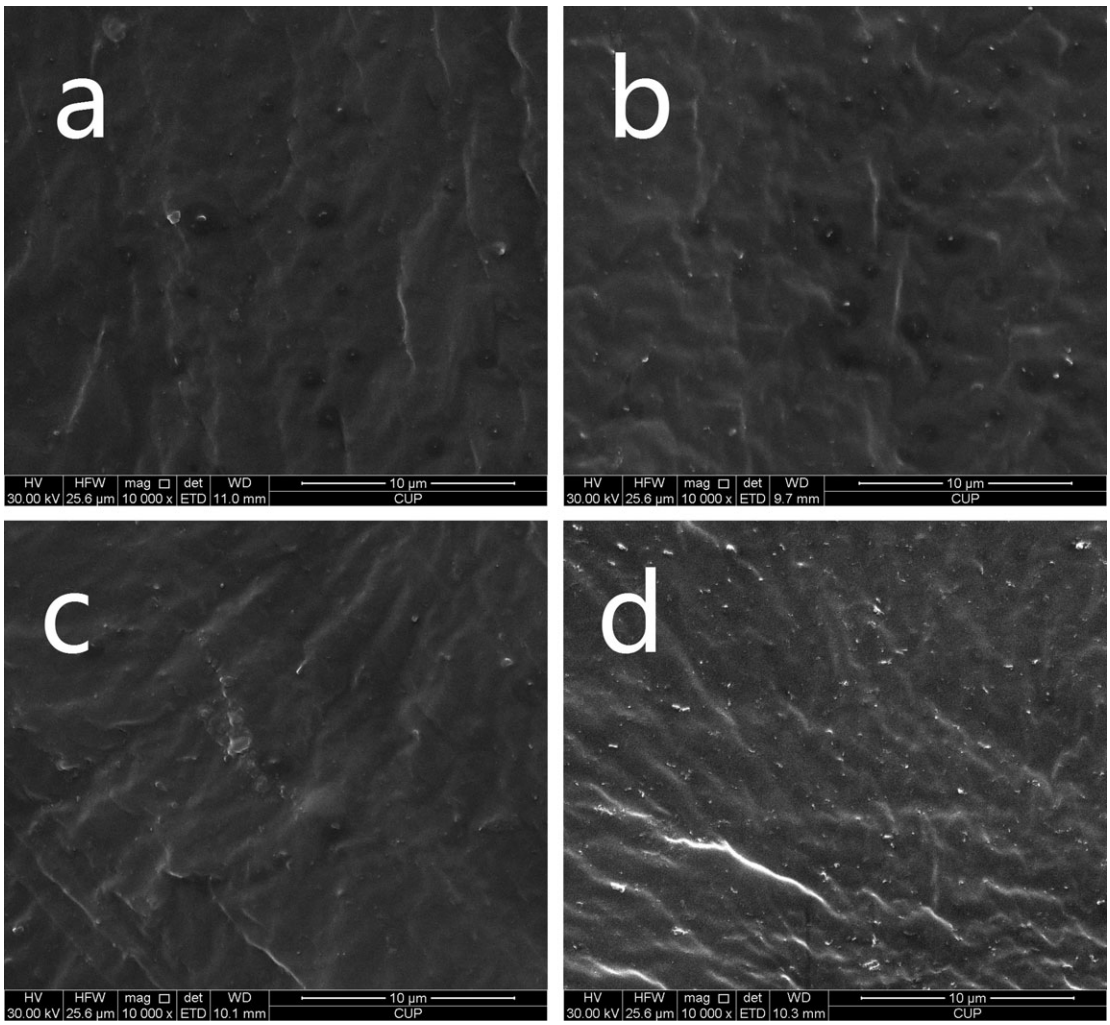

Figure 5. SEM images of the TFE/P-POSS composites with different POSS contents: (a) POSS-2, (b) POSS-4, (c) POSS-6, and (d) POSS-8.

Applied Polymer SCIENCE

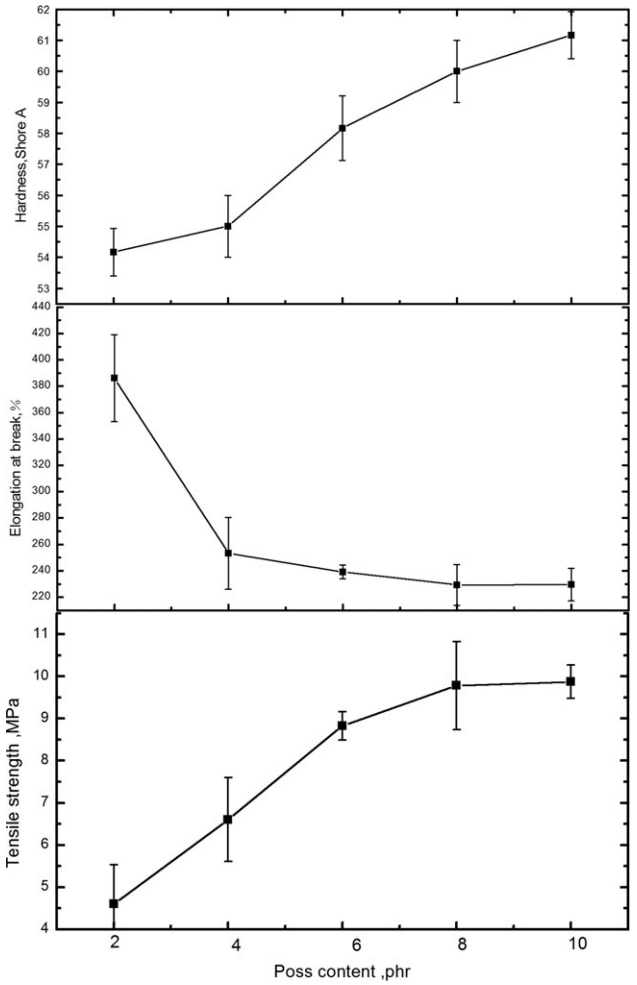

Figure 6. Mechanical properties of the TFE/P-POSS composites with different OVPOSS loadings.

II. The T_{dec} of pure rubber is 436°C, and pure rubber has nearly no remnant when the temperature reaches 700°C. The T_{dec} of pure POSS is 230°C and has 5.78% remnant. For the TEF/P-

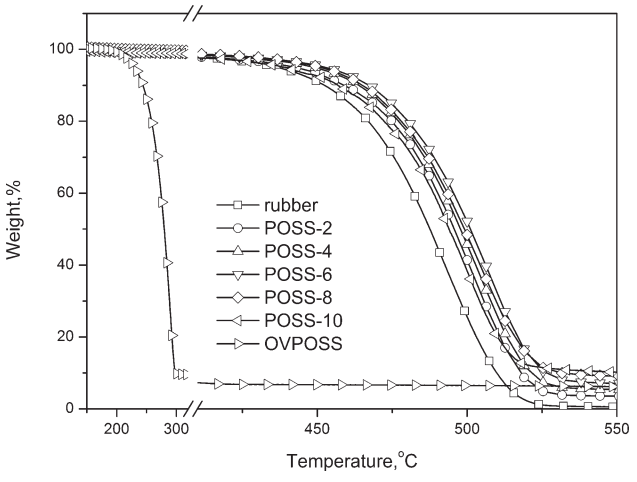

Figure 7. TGA thermograms of the TFE/P-POSS composites with different OVPOSS loadings.

Table II. TGA Parameters of the TFE/P-POSS Composites with Different OVPOSS Contents

Samples	T_{dec} (°C)	Experimental char yield, %	Theoretical char yield, %
Rubber	436	0.17	0.17
POSS-2	436	3.27	0.28
POSS-4	445	4.86	0.39
POSS-6	451	6.38	0.51
POSS-8	448	8.20	0.62
POSS-10	406	8.30	0.73
OVPOSS	230	5.78	5.78

POSS composites, the incorporation of POSS can obviously enhance the thermal property of the TFE/P rubber, although the T_{dec} of pure OVPOSS is 230°C. The T_{dec} and char yield of the TFE/P-POSS composites vary with OVPOSS loading. POSS-6 reaches its maximum T_{dec} at 451°C, and POSS-10 reaches its maximum char yield at 8.3%. This result is attributed to the fact that low OVPOSS loading increases crosslink without aggregation and that high OVPOSS loading causes aggregation, which deteriorates the thermal property of the composites. The rate of increase in T_{dec} in the present study is smaller than that in previous studies on other polymer composites.[26,29] Generally, the char yield of the composites is smaller than that of OVPOSS but larger than that of rubber because the char yield of OPOSS is large but that of rubber is small. However, the char yield of the composites is higher than that of pure OVPOSS when the OVPOSS loading is up to 6 phr. To clarify the change, the theoretical char yield is calculated in Table II based on the hypothesis that the char yield is proportional to the composite ingredients. The experimental char yield of the composites is obviously larger than the theoretical char yield, indicating that more complicated reactions occur during heat decomposition in nitrogen environment. A similar phenomenon was observed by previous studies.[22,23] However, the reason behind this phenomenon remains unknown. The changes in T_{dec} and char yield may be attributed to the formation of sour chemicals, such as HF, during decomposition.[30] Sour chemicals can destroy the ceramic coating that should form in other polymer-POSS composites.[31] The high char yield suggests that the ceramic coating may be converted into other inorganic materials, rather than SiO_2, which forms during the decomposition of pure OVPOSS.[31] The new decomposition production is heavier than SiO_2. The decomposition products of the composites need to be further characterized. In addition, the decomposition mechanisms of the composites should be explored further.

The TFE/P-POSS composites are also evaluated using DMA, and the results are showed in Figure 8. The spectra of loss factor tanδ display only one relaxation process corresponding to the glass transition of the composites with different POSS loadings. The DMA glass transition temperatures (T_g) are listed in Table III. The DMA results are consistent with the DSC results. The T_g value of DMA is slightly higher than that of DSC

Table III. Dynamic Mechanical Analysis of the OVPOSS-TFE/P Composites

Sample	Peak values of tan δ at T_g	T_g (DMA), °C	T_g (DSC), °C
POSS-2	0.72	2.4	−6.3
POSS-4	0.93	3.1	−5.9
POSS-6	0.81	4.5	−5.6
POSS-8	0.81	9.5	−4.7

because the former is more sensitive to large-scale molecular motions than the latter, although the two methods are both based on the thermal motions of polymer chains. The frequency applied in DMA is normally much greater than that in DSC, causing the T_g of DMA to shift to a higher temperature.[32] The increase in T_g of the composites is attributed to the chain mobility limit for the interaction between the macromolecules and OVPOSS cages. The peak values of tanδ in Table III show a maximum point of POSS-4 at 0.93. A small amount of OVPOSS can elevate the peak value of tanδ to increase the crosslink density of the rubber matrix. The excessive addition of POSS causes the aggregation of POSS cages, which do not contribute to mechanical loss.

CONCLUSIONS

TFE/P can be vulcanized by DCP/OVPOSS, while OVPOSS functions as an auxiliary crosslinking agent. The vinyl groups of OVPOSS participate in the crosslink reaction with TFE/P. With increasing POSS content, the crosslink density increases and the utilization ratio of vinyl groups, which function as cross-linking reaction functional groups, decreases. This result coincides with the result that OVPOSS aggregates when OVPOSS usage reaches 6 phr, as characterized by SEM and XRD. OVPOSS significantly enhances the mechanical properties and elevates the glass temperature of the composites. However, the thermal endurance properties are only improved slightly. Therefore, the potential of the curing system to improve the working performance of the composites under special working conditions will be given more focus in our future works.

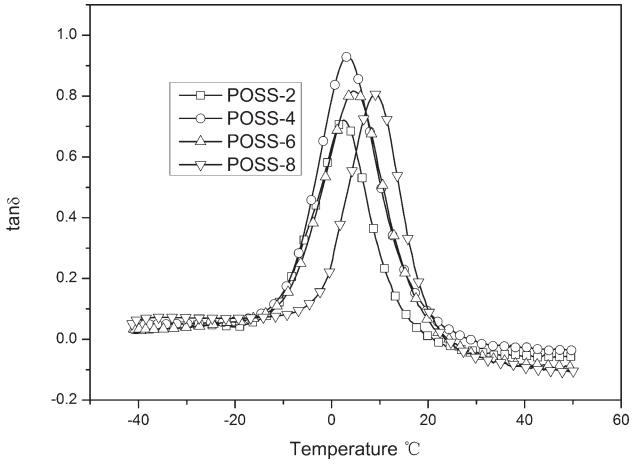

Figure 8. Dynamic mechanical spectra of the OVPOSS-TFE/P composites with different OVPOSS loadings.

ACKNOWLEDGMENTS

This work was supported by National Science Fund of China (51003121) , Cultivation Fund of the Key Scientific and Technical Innovation Project, Ministry of Education of China (NO 707010), Important National Science & Technology Specific Projects(2008ZX05017-003-03-01HZ), and China Petrochemical Corporation.

REFERENCES

1. Kostov, G. *J. Fluorine Chem.* **1985**, *29*(1–2), 109.
2. Kostov, G. K.; Chr Petrov, P. *J. Polym. Sci. Part A: Polym. Chem.* **1992**, *30*, 1083.
3. Kulkarni, S. B.; Kariduraganavar, M. Y.; Aminabhavi, T. M. *J. Appl. Polym. Sci.* **2003**, *89*, 3201.
4. Logothetis, A. L. *Prog. Polym. Sci.* **1989**, *14*, 251.
5. Bolln, C., Tsuchida, A.; Frey, H.; Mülhaupt, R. *Chem. Mater.* **1997**, *9*, 1475.
6. Anderson, S. E., Mitchell, C.; Haddad, T. S.; Vij, A.; Schwab, J. J.; Bowers, M. T. *Chem. Mater.* **2006**, *18*, 1490.
7. Qu, Y., Huang, G. S.; Wang, X. A; Li, J. L. *J. Appl. Polym. Sci.* **2012**, *125*, 3658.
8. Zhang, Z., Liang, G. Z.; Fang, C. Q.; Pei, J. Z.; Chen, S. F. *J. Appl. Polym. Sci.* **2012**, *125*, 2281.
9. Zhang, R., Shi, Z. X.; Liu, Y.; Yin, J. *J. Appl. Polym. Sci.* **2012**, *125*, 3191.
10. Wang, H., Wang, X. F.; Wang, X. Z.; Tang, L.; Wei, Y. *Mater. Rev.* **2012**, *26*(3A), 144.
11. Ye, Y.-S., Shen, W. C.; Tseng, C. Y.; Rick, J.; Huang, Y. J.; Chang, F. C.; Hwang, B. J. *Chem. Commun.* **2011**, *47*, 10656.
12. Li, Y., Dong, X. H.; Guo, K.; Wang, Z.; Chen, Z.; Wesdemiotis, C.; Quirk, R. P.; Zhang, W. -B.; Cheng, S. Z. D. *Acs Macro Lett.* **2012**, *1*, 834.
13. Zhang, W., Li, X.; Li, L.; Yang, R. *Polym. Degrad. Stabil.* **2012**, *97*, 1041.
14. Wang, X., Xuan, S.; Song, L.; Yang, H.; Lu, H.; Hu, Y. *J. Macromol. Sci. Part B-Phys.* **2012**, *51*(1–3), 255.
15. Miltner, H. E., Watzeels, N.; Gotzen, N. -A.; Goffin, A. L.; Duquesne, E.; Benali, S.; Ruelle, B.; Peeterbroeck, S.; Dubois, P.; Goderis, B.; Van Assche, G.; Rahier, H.; Van Mele, B. *Polymer* **2012**, *53*, 1494.
16. Li, L.; Li, X.; Yang, R. *J. Appl. Polym. Sci.* **2012**, *124*, 3807.
17. Zeng, L., Liang, G. Z; Gu, A. J.; Yuan, L.; Zhuo, D. X.; Hu, J. T. *J. Mater. Sci.* **2012**, *47*, 2548.
18. Chen, D.; Liu, Y.; Huang, C. *Polym. Degrad. Stabil.* **2012**, *97*, 308.
19. Yu, J., Huang, X. Y.; Wu, C.; Wu, X. F.; Wang, G. L.; Jiang, P. K. *Polymer* **2012**, *53*, 471.
20. Zhang, Q., He, H.; Xi, K.; Huang, X.; Yu, X. H.; Jia, X. D. *Macromolecules* **2011**, *44*, 550.
21. Guo, B., Lei, Y. D.; Chen, F.; Liu, X. L.; Du, M. L.; Jia, D. *Appl. Surface Sci.* **2008**, *255*, 2715.

22. Feng, Y., Jia, Y.; Guang, S.Y.; Xu, H.Y. *J. Appl. Polym. Sci.* **2010**, *115*, 2212.
23. Yang, B., Li, J. R.; Wang, J. F.; Xu, H. Y.; Guang, S. Y.; Li, C. *J. Appl. Polym. Sci.* **2009**, *111*, 2963.
24. Zhao, H., Shu, J.; Chen, Q.; Zhang, S. M. *Solid State Nuclear Magnetic Resonance* **2012**, *43*, 56.
25. Xu, H., Yang, B. H.; Wang, J. F.; Guang, S. Y.; Li, C. *J. Polym. Sci. Part a-Polym. Chem.* **2007**, *45*, 5308.
26. Yang, B., Xu, H.; Wang, J.; Gang, S.; Li, C. *J. Appl. Polym. Sci.* **2007**, *106*, 320.
27. Wang, W., Jie, X. X.; Fei, M.; Jiang, H. *J. Polym. Res.* **2011**, *18*, 13.
28. Li, H., Zhang, J. Y.; Xu, R. W; Yu, D. S. *J. Appl. Polym. Sci.* **2006**, *102*, 3848.
29. Sheen, Y.-C., Lu, C. H.; Huang, C. F.; Kuo, S. W.; Chang, F. C. *Polymer* **2008**, *49*, 4017.
30. Schild, H. G. *J. Polym. Sci. Part A: Polym. Chem.* **1993**, *31*, 1629.
31. Fina, A., Tabuani, D.; Carniato, F.; Frache, A.; Boccaleri, E.; Camino, G. *Thermochimica Acta* **2006**, *440*, 36.
32. Cho, D.; Choi, Y.; Drzal, L. T. *Polymer* **2001**, *42*, 4611.